PHYSICAL REVIEW D **80,** 093004 (2009)

One vanishing minor in the neutrino mass matrix

E. I. Lashin[1,2,3,*] and N. Chamoun[4,5,†]

[1]*The Abdus Salam ICTP, P.O. Box 586, 34100 Trieste, Italy*
[2]*Ain Shams University, Faculty of Science, Cairo 11566, Egypt*
[3]*Department of Physics and Astronomy, College of Science, King Saud University, Riyadh, Saudi Arabia*
[4]*Physics Department, HIAST, P.O. Box 31983, Damascus, Syria*
[5]*Centro Brasileiro de Pesquisas Fisicas, Rua Dr Xavier Sigaud 150, Rio de Janeiro, Brazil*

(Received 7 October 2009; published 20 November 2009)

We study a specific texture of the neutrino mass matrix, namely the models with one 2×2 subdeterminant equal to zero. We carry out a complete phenomenological analysis with all possible relevant correlations. Every pattern of the six possible ones is found able to accommodate the experimental data, with three cases allowing also for noninvertible mass matrices. We present symmetry realizations for all the models.

DOI: 10.1103/PhysRevD.80.093004 PACS numbers: 14.60.Pq, 11.30.Hv, 14.60.St

I. INTRODUCTION

Massive neutrinos and flavor mixing are the common ingredients in the interpretation of the Super-Kamiokande [1] experiment on the solar and atmospheric neutrinos. In the flavor basis which identifies the flavor eigenstates of the charged leptons with their mass eigenstates, the (effective) neutrino mass matrix M_ν has nine free parameters: three masses (m_1, m_2, and m_3), three mixing angles (θ_x, θ_y, and θ_z) and three phases (two Majorana-type ρ, σ and one Dirac-type δ). The values of the masses and the mixing angles are, somehow, constrained by data [2–5], whereas the phases are completely unrestricted by current data.

Many viable zero textures were studied. No three independent zeros texture can accommodate the data, whereas nine patterns of two independent zeros texture, out of 15 possible, can do this [6,7]. A specific model realizing any of the possible six patterns of one zero texture is constructed in [8], however, it led always to noninvertible mass matrices, some of which are compatible with current data.

The seesaw mechanism relates M_ν to the Dirac neutrino mass matrix M_D and the Majorana mass matrix of the right-handed singlet neutrinos M_R through

$$M_\nu = M_D M_R^{-1} M_D^T, \tag{1}$$

A zero in the inverted mass matrix M_ν^{-1}, when it exists, is related to a zero in M_R, when M_D is diagonal. In this respect, symmetry realizations of zeros in M_R [9] leading to zero textures in M_ν^{-1} were studied in [10], and seven patterns of two zeros texture in M_ν^{-1} were shown to be viable. However, these textures do not apply in the case of noninvertible M_ν where the zeros in M_R reflect themselves only as zero minors of M_ν. For this, the class of two independent zero minors textures in M_ν, irrespective of being invertible or not, were investigated in [11]. Seven patterns could accommodate the data, with some viable textures allowing for singular mass matrix with m_3 and θ_z equal to zero.

One can generalize the zero textures in M_ν in other ways. For instance, textures of vanishing two subtraces were tackled in [12] and eight patterns were acceptable phenomenologically. In this paper, we apply the phenomenological analysis of [11–13] to study the textures of one vanishing minor in M_ν, without presupposing the invertibility of M_ν nor assuming any specific model, albeit we showed possible theoretical realizations of the patterns.

With the vanishing constraint (two real conditions) and the input of $\Delta m^2_{\rm sol}$ fixed to its experimental central value, one still needs to know six parameters in order to determine the mass matrix. We take the mixing and phase angles to be these parameters, and so we vary the values of the mixing angles θ_x, θ_y, and θ_z over their allowed experimental ranges whereas the unconstrained phase angles δ, ρ, and σ span their whole ranges. In this manner, one can obtain in the parameter space of θ_x, θ_y, θ_z, δ, ρ, and σ the regions that are consistent with all other experimental constraints. Moreover, one can study the correlations between any two physical neutrino parameters x and y by plotting all the points (x, y) corresponding to acceptable points in the parameter space. We found that all six patterns, with three among them allowing for zero m_3, could accommodate the data. Furthermore, four patterns exhibit all sorts of neutrino mass hierarchies, whereas one pattern allows solely for an inverted hierarchy in contrast to another pattern showing only normal and degenerate hierarchies.

The plan of the paper is as follows: in Sec. II, we review the standard notation for the neutrino mass matrix and its relation to the experimental constraints. In Sec. III, we present the texture of one vanishing minor in M_ν and find the corresponding expressions of the two neutrino mass ratios. In Sec. IV, we classify all the patterns and present the results and the phenomenological analysis of

*elashin@ictp.it
†nchamoun@hiast.edu.sy

each case. We present symmetry realizations of all models in Sec. V and end up with conclusions in Sec. VI.

II. STANDARD NOTATION

In the flavor basis, which diagonalizes the charged lepton mass matrix, the symmetric neutrino mass matrix M_ν can be diagonalized by a unitary transformation,

$$V^\dagger M_\nu V^* = \begin{pmatrix} m_1 & 0 & 0 \\ 0 & m_2 & 0 \\ 0 & 0 & m_3 \end{pmatrix}, \tag{2}$$

with m_i (for $i = 1, 2, 3$) real and positive. We introduce the mixing angles $(\theta_x, \theta_y, \theta_z)$ and the phases (δ, ρ, σ) such that [7]

$$V = UP \tag{3}$$

$$P = \mathrm{diag}(e^{i\rho}, e^{i\sigma}, 1) \tag{4}$$

$$U = \begin{pmatrix} c_x c_z & s_x c_z & s_z \\ -c_x s_y s_z - s_x c_y e^{-i\delta} & -s_x s_y s_z + c_x c_y e^{-i\delta} & s_y c_z \\ -c_x c_y s_z + s_x s_y e^{-i\delta} & -s_x c_y s_z - c_x s_y e^{-i\delta} & c_y c_z \end{pmatrix} \tag{5}$$

(with $s_x \equiv \sin\theta_x \ldots$). We then have

$$M_\nu = U \begin{pmatrix} \lambda_1 & 0 & 0 \\ 0 & \lambda_2 & 0 \\ 0 & 0 & \lambda_3 \end{pmatrix} U^T \tag{6}$$

with

$$\lambda_1 = m_1 e^{2i\rho}, \qquad \lambda_2 = m_2 e^{2i\sigma}, \qquad \lambda_3 = m_3. \tag{7}$$

In this parametrization, the mass matrix elements are given by

$$\begin{aligned}
M_{\nu 11} &= m_1 c_x^2 c_z^2 e^{2i\rho} + m_2 s_x^2 c_z^2 e^{2i\sigma} + m_3 s_z^2, \\
M_{\nu 12} &= m_1(-c_z s_z c_x^2 s_y e^{2i\rho} - c_z c_x s_x c_y e^{i(2\rho-\delta)}) + m_2(-c_z s_z s_x^2 s_y e^{2i\sigma} + c_z c_x s_x c_y e^{i(2\sigma-\delta)}) + m_3 c_z s_z s_y, \\
M_{\nu 13} &= m_1(-c_z s_z c_x^2 s_y e^{2i\rho} + c_z c_x s_x s_y e^{i(2\rho-\delta)}) + m_2(-c_z s_z s_x^2 c_y e^{2i\sigma} - c_z c_x s_x s_y e^{i(2\sigma-\delta)}) + m_3 c_z s_z c_y, \\
M_{\nu 22} &= m_1(c_x s_z s_y e^{i\rho} + c_y s_x e^{i(\rho-\delta)})^2 + m_2(s_x s_z s_y e^{i\sigma} - c_y c_x e^{i(\sigma-\delta)})^2 + m_3 c_z^2 s_y^2, \\
M_{\nu 33} &= m_1(c_x s_z c_y e^{i\rho} - s_y s_x e^{i(\rho-\delta)})^2 + m_2(s_x s_z c_y e^{i\sigma} + s_y c_x e^{i(\sigma-\delta)})^2 + m_3 c_z^2 c_y^2, \\
M_{\nu 23} &= m_1(c_x^2 c_y s_y s_z^2 e^{2i\rho} + s_z c_x s_x (c_y^2 - s_y^2) e^{i(2\rho-\delta)} - c_y s_y s_x^2 e^{2i(\rho-\delta)}) + m_2(s_x^2 c_y s_y s_z^2 e^{2i\sigma} + s_z c_x s_x (s_y^2 - c_y^2) e^{i(2\sigma-\delta)} \\
&\quad - c_y s_y c_x^2 e^{2i(\sigma-\delta)}) + m_3 s_y c_y c_z^2.
\end{aligned} \tag{8}$$

We see here that under the transformation given by

$$T_1\colon \theta_y \to \frac{\pi}{2} - \theta_y \quad \text{and} \quad \delta \to \delta \pm \pi, \tag{9}$$

the mass matrix elements are transformed among themselves such that the indices 2 and 3 are swapped under T_1 whereas the index 1 remains invariant:

$$\begin{aligned}
&M_{\nu 11} \leftrightarrow M_{\nu 11}, \qquad M_{\nu 12} \leftrightarrow M_{\nu 13} \\
&M_{\nu 22} \leftrightarrow M_{\nu 33}, \qquad M_{\nu 23} \leftrightarrow M_{\nu 23}.
\end{aligned} \tag{10}$$

There is another symmetry given by

$$T_2\colon \rho \to \pi - \rho, \qquad \sigma \to \pi - \sigma, \qquad \delta \to 2\pi - \delta, \tag{11}$$

which changes the mass matrix into its complex conjugate, i.e.,

$$M_{\nu ij}(T_2(\delta, \rho, \sigma)) = M^*_{\nu ij}((\delta, \rho, \sigma)). \tag{12}$$

The above two symmetries $T_{1,2}$ are very useful in classifying the models and in connecting the phenomenological analysis of patterns related by these symmetries.

A remarkable merit of this parametrization is that its mixing angles $(\theta_x, \theta_y, \theta_z)$ are directly related to the mixing angles of solar, atmospheric, and CHOOZ reactor neutrino oscillations:

$$\theta_x \approx \theta_{\mathrm{sol}}, \qquad \theta_y \approx \theta_{\mathrm{atm}}, \qquad \theta_z \approx \theta_{\mathrm{chz}}. \tag{13}$$

Also, we have

$$\begin{aligned}
\Delta m^2_{\mathrm{sol}} &= \Delta m^2_{12} = m_2^2 - m_1^2, \\
\Delta m^2_{\mathrm{atm}} &= |\Delta m^2_{23}| = |m_3^2 - m_2^2|,
\end{aligned} \tag{14}$$

and the hierarchy of solar and atmospheric neutrino mass-squared differences is characterized by the parameter:

$$R_\nu \equiv \left| \frac{m_2^2 - m_1^2}{m_3^2 - m_2^2} \right| \approx \frac{\Delta m^2_{\mathrm{sol}}}{\Delta m^2_{\mathrm{atm}}} \ll 1. \tag{15}$$

Reactor nuclear experiments on beta-decay kinematics and neutrinoless double-beta decay put constraints on the neutrino mass scales characterized by the effective electron-neutrino mass:

$$\langle m\rangle_e = \sqrt{\sum_{i=1}^{3}(|V_{ei}|^2 m_i^2)}, \tag{16}$$

and the effective Majorana mass term $\langle m\rangle_{ee}$:

$$\langle m\rangle_{ee} = |m_1 V_{e1}^2 + m_2 V_{e2}^2 + m_3 V_{e3}^2| = |M_{\nu 11}|^2. \tag{17}$$

The Jarlskog rephasing invariant quantity [14] that measures CP violation in neutrino oscillation is given by

$$J = s_x c_x s_y c_y s_z c_z^2 \sin\delta. \tag{18}$$

Also, cosmological observations put an upper bound on the "sum" parameter Σ:

$$\Sigma = \sum_{i=1}^{3} m_i. \tag{19}$$

There are no experimental bounds on the phase angles, and we take the principal value range for δ, 2ρ, and 2σ to be $[0, 2\pi]$. As to the other oscillation parameters, the experimental constraints give the following values with 1, 2, and 3 $-$ σ errors [13,15]:

$$\begin{aligned} \Delta m^2_{\rm atm} &= 2.6^{+0.2,0.4,0.6}_{-0.2,0.4,0.6} \times 10^{-3}\ \text{eV}^2, \\ \Delta m^2_{\rm sol} &= 7.9^{+0.3,0.6,1.0}_{-0.3,0.6,0.8} \times 10^{-5}\ \text{eV}^2, \end{aligned} \tag{20}$$

$$\begin{aligned} \sin^2\theta_{\rm atm} &= (0.5^{+0.05,0.13,0.18}_{-0.05,0.12,0.16}) \leftrightarrow \theta_y \\ &= (45^{+3.44,7.54,10.55}_{-2.87,6.95,9.34})\ \text{degree}, \\ \sin^2\theta_{\rm sol} &= (0.3^{+0.02,0.06,0.10}_{-0.02,0.04,0.06}) \leftrightarrow \theta_x \\ &= (33.21^{+1.24,3.66,6.02}_{-1.27,2.56,3.88})\ \text{degree}, \\ \sin^2\theta_{\rm chz} &< 0.012, 0.025, 0.040 \\ &\leftrightarrow \theta_z < (6.29, 9.10, 11.54)\ \text{degree}. \end{aligned} \tag{21}$$

The most stringent condition on any model required to fit the data is the bound on the R_ν parameter:

$$R_\nu = (0.0304^{+0.0038,0.0082,0.0141}_{-0.0033,0.0061,0.0082}). \tag{22}$$

Concerning the nonoscillation parameters $\langle m\rangle_e$, Σ, and $\langle m\rangle_{ee}$, we adopt the 2 $-$ σ bounds for both $\langle m\rangle_e$ and Σ as reported in [15]:

$$\langle m\rangle_e < 1.8\ \text{eV}, \qquad \Sigma < 1.4\ \text{eV}. \tag{23}$$

Due, in large part, to the debate about the claimed observation of neutrinoless double beta decay, we left in our phenomenological analysis the effective Majorana mass term $\langle m\rangle_{ee}$ unconstrained.

III. NEUTRINO MASS MATRICES WITH ONE VANISHING MINOR

We denote by C_{ij} the minor corresponding to the ijth element (i.e. the determinant of the submatrix obtained by deleting the ith row and the jth column of M_ν). We have six possibilities of having one minor vanishing. The vanishing minor condition is written as

$$M_{\nu ab} M_{\nu cd} - M_{\nu ij} M_{\nu mn} = 0, \tag{24}$$

then we have

$$\sum_{l,k=1}^{3} (U_{al} U_{bl} U_{ck} U_{dk} - U_{il} U_{jl} U_{mk} U_{nk}) \lambda_l \lambda_k = 0. \tag{25}$$

This leads to

$$\frac{m_1}{m_3} = \frac{\text{Re}(A_2 e^{-2i\sigma})\text{Im}(A_1 e^{-2i\rho}) - \text{Re}(A_1 e^{-2i\rho})\text{Im}(A_2 e^{-2i\sigma})}{\text{Re}(A_3)\text{Im}(A_2 e^{-2i\sigma}) - \text{Re}(A_2 e^{-2i\sigma})\text{Im}(A_3)} \tag{26}$$

$$\frac{m_2}{m_3} = \frac{\text{Re}(A_2 e^{-2i\sigma})\text{Im}(A_1 e^{-2i\rho}) - \text{Re}(A_1 e^{-2i\rho})\text{Im}(A_2 e^{-2i\sigma})}{\text{Re}(A_1 e^{-2i\rho})\text{Im}(A_3) - \text{Re}(A_3)\text{Im}(A_1 e^{-2i\rho})}, \tag{27}$$

where

$$A_h = (U_{al} U_{bl} U_{ck} U_{dk} - U_{il} U_{jl} U_{mk} U_{nk}) + (l \leftrightarrow k), \tag{28}$$

where (h, l, k) are a cyclic permutation of (1, 2, 3).

One can compute the analytical expressions, in terms of (θ_x, θ_y, θ_z, δ, ρ, and σ), of all the quantities measured experimentally. In order to explore the parameter space of these six parameters, we have spanned the mixing angles θ_x, θ_y, and θ_z over their experimentally allowed ranges given in Eq. (21), while the phases ρ, σ, and δ were varied in their full ranges. With $\Delta m_{\rm sol}$ equal to its central value, we determined in the parameter space the acceptable regions compatible with the other experimental constraints given by Eqs. (20), (22), and (23). One can then illustrate graphically all the possible correlations, in the three levels of σ error, between any two physical neutrino parameters. We chose to plot for each pattern and for each type of hierarchy 26 correlations at the 2σ error level involving the parameters (m_1, m_2, m_3, θ_x, θ_y, θ_z, ρ, σ, δ, J, m_{ee}) and the lowest neutrino mass (LNM). Moreover, for each parameter, one can determine the extremum values it can take according to the considered precision level, and we listed in the tables these predictions for all the patterns and for the three σ-error levels.

We found that the resulting mass patterns could be classified into three categories:

(i) Normal hierarchy: characterized by $m_1 < m_2 < m_3$ and is denoted by **N**. For this type of hierarchy, we imposed numerically the bound:

$$\frac{m_1}{m_3} < \frac{m_2}{m_3} < 0.7. \tag{29}$$

(ii) Inverted hierarchy: characterized by $m_3 < m_1 < m_2$ and is denoted by **I**. We imposed the corresponding bound:

$$\frac{m_2}{m_3} > \frac{m_1}{m_3} > 1.3. \tag{30}$$

(iii) Degenerate hierarchy: characterized by $m_1 \approx m_2 \approx m_3$ and is denoted by **D**. The corresponding numeric bound was taken to be

$$0.7 < \frac{m_1}{m_3} < \frac{m_2}{m_3} < 1.3. \tag{31}$$

Also, one should investigate the possibility, for each pattern, to have singular (noninvertible) mass matrix. The viable singular mass matrix is characterized by one of the masses (m_1, m_2, and m_3) being equal to zero, as compatibility with the data prevents the simultaneous vanishing of two masses and even vanishing of m_2 alone:

- The vanishing of m_1 implies that $A_1 = 0$ and the mass spectrum of m_2 and m_3 takes the values $\sqrt{\Delta m^2_{\rm sol}}$ and $\sqrt{\Delta m^2_{\rm sol} + \Delta m^2_{\rm atm}}$, respectively.
- The vanishing of m_3 implies that $A_3 = 0$ and the mass spectrum of m_2 and m_1 takes the values $\sqrt{\Delta m^2_{\rm atm}}$ and $\sqrt{\Delta m^2_{\rm atm} - \Delta m^2_{\rm sol}}$, respectively.

The symmetry T_1 introduced in Eqs. (9) and (10) induces equivalence between different patterns of vanishing one minor as $C_{33} \leftrightarrow C_{22}$, and $C_{31} \leftrightarrow C_{21}$. One should, however, keep in mind that this equivalence for θ_y is a reflection about the first bisectrix, i.e. it maps the θ_y from the first octant to the second octant and vice versa. Similarly, the image points of the map differ in δ from their original points by a shift equal to π. This means that the accepted points for a pattern imply for the equivalent pattern the same accepted points but after changing the θ_y and δ correspondingly.

Thus, it suffices now to present four possible cases, instead of six, corresponding to one vanishing minor in M_ν. Since the analytical expressions in terms of (θ_x, θ_y, θ_z, δ, ρ, and σ) are quite complicated, we state, simple writing permitting, only the leading terms of the expansions in powers of s_z.

IV. RESULTS OF TEXTURES WITH ONE VANISHING MINOR

In this section, we shall present the results of our numerical analysis for the four possible independent models based upon the approach described in the previous section. The coefficients $A's$ [Eq. (28)] defining each model are presented. In order to get some interpretation of the numerical results, we present also the analytical expressions of the mass ratios up to leading order in s_z, except in the last pattern C_{11} where we give the full, relatively simple, analytical expressions of the mass ratios and other experimental parameters.

We organized the large number of correlation figures in plots, at the 2σ-error level, by dividing, where applicable, each figure into left and right panels denoted accordingly by the letters L and R. Additional labels (D, N, and I) are attached to the plots to indicate the type of hierarchy (Degenerate, Normal and Inverted, respectively). Any missing label D, N, or I on the figures of certain model would mean the absence of the corresponding hierarchy type in this model.

We listed in Tables I and II, for the three types of hierarchy and the three precision levels, the extremum values that the different parameters can take. The corresponding ranges should get larger with higher-σ precision levels. However, these bounds were evaluated by spanning the parameter space with some given number [of order (10^8–10^9)] of points chosen randomly in the parameter space. We found this way of random spanning more efficient than a regular meshing with nested loops. For a regular meshing with a fixed step of ''modest'' order of 1°, we need around 10^{10} points to cover the experimentally allowed space. However, in order to be efficient, the spanning needs a ''dynamic'' step for a finer meshing in the regions full of accepted points compensated by less spanning in the disallowed regions. With the random spanning we do not have this problem. Moreover, the randomness of our spanning allowed us to check the stability of our results for different randomly chosen points when we ran the programs several times. Thus, the values in the tables are meant to give only a strong qualitative indication. In particular, an attainable zero value for θ_z at one level implies this value is attainable for all higher σ levels, even though the corresponding values in the tables might be slightly larger than zero.

A. Pattern of vanishing minor C_{33}; $M_{\nu 11}M_{\nu 22} - M_{\nu 12}M_{\nu 12} = 0$

In this model, the relevant expressions for A_1, A_2, and A_3 are

$$\begin{aligned} A_1 &= (s_x s_y - s_z c_x c_y e^{-i\delta})^2, \\ A_2 &= (c_x s_y + s_z s_x c_y e^{-i\delta})^2, \\ A_3 &= c_z^2 c_y^2 e^{-2i\delta}, \end{aligned} \tag{32}$$

leading to

$$\frac{m_1}{m_3} \approx \frac{s_x^2 t_y^2 s_{2\rho-2\sigma}}{s_{2\sigma-2\delta}} + O(s_z) \tag{33}$$

$$\frac{m_2}{m_3} \approx \frac{c_x^2 t_y^2 s_{2\rho-2\sigma}}{s_{2\delta-2\rho}} + O(s_z). \tag{34}$$

In the left panel of Fig. 1, we present the correlations of the angle δ against the mixing angles (θ_x, θ_y, θ_z), the CP phases (ρ, σ), and the Jarlskog invariant quantity J,

TABLE I. The various predictions for the models of one-vanishing minor C_{33}, C_{22}, and C_{31}. The minor corresponding to the index (ij) is the determinant of the submatrix obtained by deleting the ith line and the jth column. All the angles (masses) are evaluated in degrees (eV). The mark $\times$ indicates that the corresponding pattern with the specified hierarchy type cannot accommodate the experimental data at the given σ precision level.

Model C_{33}: $M_{\nu 11}M_{\nu 22} - M_{\nu 12}M_{\nu 12} = 0$

Quantity	θ_x	θ_y	θ_z	m_1	m_2	m_3	ρ	σ	δ	$\langle m\rangle_e$	$\langle m\rangle_{ee}$	J
Degenerate hierarchy												
1σ	31.94–34.45	42.13–48.44	0.0003–6.28	0.0489–0.4029	0.0497–0.4030	0.0659–0.3997	0.0780–179.83	0.1143–179.69	0.1978–359.83	0.0493–0.4029	0.0222–0.3754	−0.0251–0.0246
2σ	30.65–36.86	39.65–52.54	0.0004–9.1	0.0471–0.4027	0.0479–0.4028	0.0567–0.3996	0.2870–179.88	0.0715–179.93	0.0554–359.90	0.0475–0.4027	0.0165–0.3309	−0.0348–0.0356
3σ	29.34–39.23	38.95–55.55	0.0008–11.53	0.0449–0.4046	0.0458–0.4047	0.0543–0.4072	0.0008–180	0.1194–180	0.3829–359.57	0.0453–0.4047	0.0097–0.2884	−0.0459–0.0455
Normal hierarchy												
1σ	31.94–34.45	42.13–48.44	0.0000–6.29	0.0019–0.0491	0.0091–0.0499	0.0499–0.0721	0.0056–179.98	0.0493–179.97	0.0307–359.87	0.0056–0.0494	0.0000–0.0422	−0.0249–0.0247
2σ	30.65–36.87	38.05–52.54	0.0025–9.1	0.0013–0.0510	0.0090–0.0518	0.0478–0.0742	0.1356–179.95	0.0515–179.99	0.1023–359.99	0.0052–0.0513	0.0000–0.0467	−0.0365–0.0359
3σ	29.33–39.23	35.66–55.55	0.0022–11.53	0.0008–0.0514	0.0089–0.0522	0.0456–0.0756	0.0465–180	0.0091–179.99	0.1535–359.99	0.0050–0.0523	0.0000–0.0449	−0.0453–0.0460
Inverted hierarchy												
1σ	$\times$	$\times$	$\times$	$\times$	$\times$	$\times$	$\times$	$\times$	$\times$	$\times$	$\times$	$\times$
2σ	30.65–36.87	48.41–52.54	0.0137–9.095	0.0575–0.0839	0.0582–0.0844	0.0339–0.0645	0.0734–179.88	0.0687–179.61	0.0338–359.66	0.0573–0.0840	0.0444–0.0831	−0.0357–0.0352
3σ	29.33–39.23	48.04–55.55	0.0003–11.54	0.0499–0.0865	0.0506–0.0870	0.0229–0.0662	0.0213–179.97	0.0095–179.96	0.1354–359.83	0.0495–0.0866	0.0300–0.0853	−0.0442–0.0442

Model C_{22}: $M_{\nu 11}M_{\nu 33} - M_{\nu 13}M_{\nu 31} = 0$

Quantity	θ_x	θ_y	θ_z	m_1	m_2	m_3	ρ	σ	δ	$\langle m\rangle_e$	$\langle m\rangle_{ee}$	J
Degenerate hierarchy												
1σ	31.94–34.45	42.13–48.44	0.0023–6.2858	0.0489–0.4563	0.0497–0.4563	0.0699–0.4593	0.0784–179.98	0.0779–179.91	0.2430–359.93	0.0494–0.4563	0.0223–0.3911	−0.0248–0.0247
2σ	30.65–36.87	38.05–50.27	0.0013–9.1	0.0469–0.4206	0.0477–0.4207	0.0575–0.4178	0.0508–179.98	0.0325–179.90	0.0793–359.81	0.0473–0.4206	0.0159–0.3269	−0.0359–0.0361
3σ	29.33–39.23	35.66–50.96	0.0007–11.53	0.0451–0.4527	0.0459–0.4528	0.0552–0.4559	0.0273–179.93	0.0474–179.95	0.2755–359.85	0.0454–0.4527	0.0109–0.3794	−0.0450–0.0456
Normal hierarchy												
1σ	31.94–34.45	42.13–48.44	0.0024–6.28	0.0017–0.0487	0.0091–0.0495	0.0499–0.0720	0.1438–179.97	0.0954–179.95	0.0441–359.73	0.0055–0.0491	0.0000–0.0397	−0.0248–0.0242
2σ	30.65–36.87	38.06–52.54	0.0004–9.1	0.0013–0.0519	0.0090–0.0527	0.0478–0.0759	0.0287–179.97	0.0578–179.97	0.0066–359.99	0.0052–0.0523	0.0000–0.0374	−0.0355–0.0359
3σ	29.33–39.23	35.66–55.55	0.0002–11.53	0.0006–0.0514	0.0089–0.0521	0.0456–0.0748	0.0168–179.97	0.0071–180	0.0304–359.98	0.0050–0.0525	0.0000–0.0454	−0.0457–0.0451
Inverted hierarchy												
1σ	$\times$	$\times$	$\times$	$\times$	$\times$	$\times$	$\times$	$\times$	$\times$	$\times$	$\times$	$\times$
2σ	30.65–36.87	38.05–41.50	0.0006–9.1	0.0582–0.0842	0.0589–0.0847	0.0352–0.0648	0.0156–179.89	0.0305–179.93	0.0713–359.80	0.0580–0.0842	0.0457–0.0826	−0.0353–0.0348
3σ	29.33–39.23	35.66–41.77	0.0021–11.53	0.0514–0.0865	0.0522–0.0869	0.0265–0.0664	0.0254–179.96	0.0049–179.87	0.1171–360	0.0510–0.0865	0.0320–0.0854	−0.0436–0.0447

Model C_{31}: $M_{\nu 12}M_{\nu 23} - M_{\nu 13}M_{\nu 22} = 0$

Quantity	θ_x	θ_y	θ_z	m_1	m_2	m_3	ρ	σ	δ	$\langle m\rangle_e$	$\langle m\rangle_{ee}$	J
Degenerate hierarchy												
1σ	31.94–34.45	42.14–48.44	0.0542–6.29	0.0493–0.2988	0.0501–0.2989	0.0593–0.2946	0.0050–179.98	0.0040–1780	0.3220–359.93	0.0495–0.2989	0.0489–0.2988	−0.0246–0.0245
2σ	30.65–36.87	38.055–52.53	0.0715–9.01	0.0473–0.4431	0.0481–0.4432	0.0569–0.4399	0.0017–179.99	0.0161–179.97	0.0778–359.83	0.0476–0.4431	0.0458–0.4368	−0.0352–0.0360
3σ	29.33–39.23	35.66–55.54	0.0705–11.54	0.0450–0.4217	0.0459–0.4217	0.0543–0.4184	0.0200–179.99	0.0040–179.99	0.0673–359.84	0.0455–0.4216	0.0395–0.4216	−0.0442–0.0453
Normal hierarchy												
1σ	31.94–34.45	42.13–48.44	0.3175–6.29	0.0092–0.0504	0.0128–0.0511	0.0509–0.0732	0.0229–179.96	0.0043–179.94	0–123 ∪ 242–360	0.0117–0.0507	0.0096–0.0506	−0.0249– − 0.0251
2σ	30.65–36.87	38.06–52.54	0.3599–9.09	0.0061–0.0521	0.0108–0.0529	0.0483–0.0760	0.0486–179.97	0.0251–179.85	0–123 ∪ 242–360	0.0105–0.0528	0.0062–0.0524	−0.0356–0.0363
3σ	29.33–39.23	35.67–55.55	0.2618–11.54	0.0047–0.0543	0.0101–0.0550	0.0462–0.0787	0.0018–179.98	0.0258–179.99	0–123 ∪ 242–360	0.0101–0.0551	0.0047–0.0538	−0.0450–0.0456
Inverted hierarchy												
1σ	31.94–34.45	42.13–48.44	0.0009–6.29	0.0482–0.0804	0.0490–0.0809	0.0000–0.0615	0.0428–180	0.0583–179.97	0.0081–359.89	0.0484–0.0804	0.0183–0.0789	−0.0246–0.0249
2σ	30.65–36.87	38.06–52.54	0.0000–9.01	0.0461–0.0809	0.0469–0.0814	0.0000–0.0620	0.0224–179.95	0.0362–179.95	0.0358–359.97	0.0463–0.0809	0.0141–0.0806	−0.0357–0.0360
3σ	29.33–39.23	35.66–55.55	0.0009–11.54	0.0439–0.0858	0.0447–0.0862	0.0000–0.0654	0.0020–179.99	0.0127–179.99	0.0026–359.94	0.0441–0.0857	0.0101–0.0848	−0.0459–0.0456

TABLE II. The various prediction for the models of one-vanishing minor C_{32}, C_{21}, and C_{11}. The minor corresponding to the index (ij) is the determinant of the submatrix obtained by deleting the ith line and the jth column. All the angles (masses) are evaluated in degrees (eV). The mark $\times$ indicates that the corresponding pattern with the specified hierarchy type cannot accommodate the experimental data at the given σ precision level.

Model C_{32}: $M_{\nu 11}M_{\nu 23} - M_{\nu 21}M_{\nu 13} = 0$												
Quantity	θ_x	θ_y	θ_z	m_1	m_2	m_3	ρ	σ	δ	$\langle m\rangle_e$	$\langle m\rangle_{ee}$	J
Degenerate hierarchy												
1σ	31.94–34.45	42.13–48.44	0.0007–6.29	0.0489–0.3459	0.0497–0.3460	0.0699–0.3495	0.0296–179.94	0.1237–180	0.0125–359.98	0.0493–0.3459	0.0336–0.3419	−0.0250–0.0248
2σ	30.66–36.87	38.05–52.54	0.0029–9.09	0.0470–0.3870	0.0478–0.3871	0.0670–0.3902	0.0101–179.83	0.0444–179.92	0.1492–359.99	0.0475–0.3870	0.0293–0.3810	−0.0362–0.0348
3σ	29.34–39.23	35.67–55.54	0.0006–11.53	0.0449–0.3765	0.0458–0.3766	0.0641–0.3738	0.0774–179.87	0.0061–180	0.0510–359.93	0.0453–0.3764	0.0232–0.3396	−0.0453–0.0459
Normal hierarchy												
1σ	31.94–34.45	42.13–48.44	0.0001–6.29	0.0029–0.0504	0.0093–0.0512	0.0499–0.0733	0.0083–179.92	0.0003–179.97	0.1523–359.99	0.0056–0.0508	0.0001–0.0352	−0.0245–0.0251
2σ	30.65–36.87	38.05–52.54	0.0019–9.1	0.0023–0.0501	0.0092–0.0509	0.0479–0.0734	0.0047–179.97	0.0596–179.99	0.0083–359.97	0.0053–0.0507	0.0000–0.0346	−0.0356–0.0366
3σ	29.33–39.23	35.66–55.55	0.0021–11.54	0.0019–0.0525	0.0091–0.0532	0.0457–0.0776	0.0185–179.99	0.0077–179.96	0.0224–360	0.0050–0.0530	0.0000–0.0365	−0.0455–0.0444
Inverted hierarchy												
1σ	×	×	×	×	×	×	×	×	×	×	×	×
2σ	×	×	×	×	×	×	×	×	×	×	×	×
3σ	×	×	×	×	×	×	×	×	×	×	×	×
Model C_{21}: $M_{\nu 21}M_{\nu 33} - M_{\nu 31}M_{\nu 23} = 0$												
Quantity	θ_x	θ_y	θ_z	m_1	m_2	m_3	ρ	σ	δ	$\langle m\rangle_e$	$\langle m\rangle_{ee}$	J
Degenerate hierarchy												
1σ	31.94–34.45	42.13–48.43	0.0386–6.29	0.0492–0.4521	0.0500–0.4521	0.0593–0.4549	0.0026–180	0.0098–179.99	0.1274–359.11	0.0494–0.4521	0.0487–0.4521	−0.0245–0.0248
2σ	30.65–36.87	38.05–52.54	0.0524–9.1	0.0470–0.4365	0.0478–0.4366	0.0568–0.4335	0.0014–180	0.0018–179.98	0.2779–359.63	0.0473–0.4365	0.0456–0.4365	−0.0362–0.0361
3σ	29.33–39.23	35.68–55.55	0.0185–11.53	0.0451–0.3307	0.0460–0.3308	0.0542–0.3272	0.0118–180	0.0003–179.98	0.5547–359.84	0.0456–0.3306	0.0402–0.3306	−0.0455–0.0455
Normal hierarchy												
1σ	31.94–34.45	42.13–48.44	0.2922–6.29	0.0096–0.0505	0.0131–0.0513	0.0508–0.0734	0.0543–179.99	0.0623–179.98	59.58–304.26	0.0120–0.0509	0.0099–0.0506	−0.0249–0.0248
2σ	30.65–36.87	38.06–52.54	0.3368–9.1	0.0062–0.0519	0.0108–0.0526	0.0483–0.0753	0.0083–179.99	0.1329–179.99	57.51–296.59	0.0108–0.0527	0.0066–0.0525	−0.0363–0.0359
3σ	29.33–39.23	35.66–55.55	0.4979–11.54	0.0050–0.0527	0.0102–0.0535	0.0460–0.0778	0.0292–179.92	0.0199–180	59.53–302.99	0.0099–0.0533	0.0048–0.0530	−0.0452–0.0457
Inverted hierarchy												
1σ	31.94–34.45	42.13–48.44	0.0000–6.29	0.0482–0.0806	0.0490–0.0810	0.0000–0.0619	0.0079–179.95	0.0857–179.96	0.1136–359.99	0.0484–0.0807	0.0180–0.0804	−0.0243–0.0246
2σ	30.65–36.87	38.05–52.54	0.0026–9.09	0.0461–0.0825	0.0469–0.0830	0.0000–0.0626	0.0076–179.96	0.0068–179.99	0.0672–359.94	0.0463–0.0824	0.0143–0.0811	−0.0356–0.0352
3σ	29.33–39.23	35.66–55.55	0.0012–11.52	0.0438–0.0849	0.0447–0.0853	0.0000–0.0650	0.0115–179.97	0.0079–179.96	0.3136–359.94	0.0440–0.0849	0.0094–0.0849	−0.0457–0.0443
Model C_{11}: $M_{\nu 22}M_{\nu 33} - M_{\nu 32}M_{\nu 23} = 0$												
Quantity	θ_x	θ_y	θ_z	m_1	m_2	m_3	ρ	σ	δ	$\langle m\rangle_e$	$\langle m\rangle_{ee}$	J
Degenerate hierarchy												
1σ	×	×	×	×	×	×	×	×	×	×	×	×
2σ	×	×	×	×	×	×	×	×	×	×	×	×
3σ	×	×	×	×	×	×	×	×	×	×	×	×
Normal hierarchy												
1σ	×	×	×	×	×	×	×	×	×	×	×	×
2σ	×	×	×	×	×	×	×	×	×	×	×	×
3σ	×	×	×	×	×	×	×	×	×	×	×	×
Inverted hierarchy												
1σ	31.94–34.45	42.13–48.44	0.0006–6.29	0.0482–0.0522	0.0490–0.0529	0.0000–0.0015	76.21–103.81	0.6212–178.88	0.0156–359.88	0.0482–0.0524	0.0177–0.0519	−0.0246–0.0248
2σ	30.65–36.87	38.05–52.54	0.0019–9.1	0.0461–0.0541	0.0469–0.0548	0.0000–0.0043	73.23–106.74	1.1273–179.71	0.0851–359.9438	0.0458–0.0543	0.0128–0.0534	−0.0357–0.0358
3σ	29.33–39.23	35.66–55.54	0.0026–11.53	0.0438–0.0562	0.0447–0.0569	0.0000–0.0088	69.51–110.52	0.6325–178.33	0.0559–359.89	0.0434–0.0560	0.0093–0.0543	−0.0452–0.0465

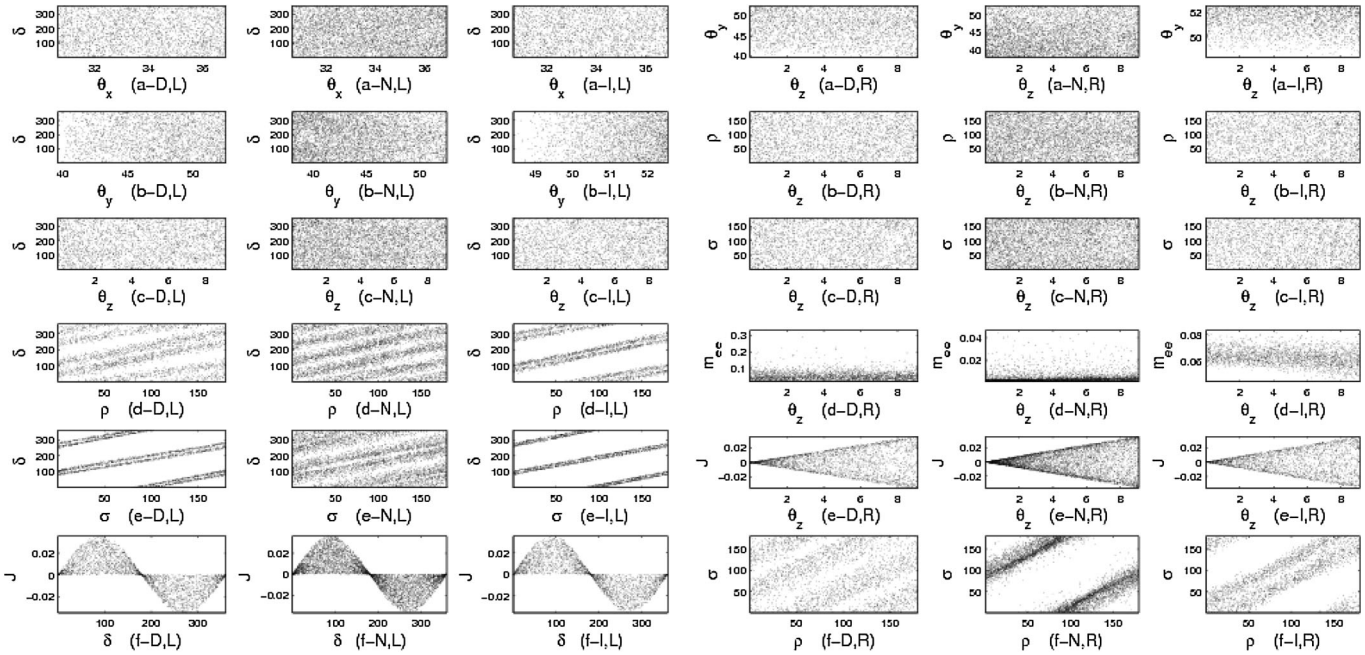

FIG. 1. Pattern $\mathbf{C}_{33}$: The left panel presents correlations of δ against mixing angles, CP phases, and J, while the right panel shows the correlations of θ_z against θ_y, ρ, σ, m_{ee}, and J, and also the correlation of ρ versus σ.

whereas in the right panel we show the correlations of θ_z against $(\theta_y, \rho, \sigma, J, \langle m\rangle_{ee})$, and the correlation of ρ versus σ.

The left panel of Fig. 2 presents five correlations of $\langle m\rangle_{ee}$ against (θ_y, δ, ρ, σ, and J) and the correlation of $m_{23} = \frac{m_2}{m_3}$ versus θ_y. As to the right panel of this figure, it presents the correlations of (ρ, σ) against θ_y and J, and those of LNM versus (ρ, J).

As to Fig. 3, and in a similar way, it presents two correlations of m_3 against $\frac{m_2}{m_3}$ and against $\frac{m_2}{m_1}$ for the three types of hierarchy. In all we have 26 types of correlations for each hierarchy type.

We see in Fig. 1 (plots: a-L $\rightarrow$ c-L, a-R $\rightarrow$ c-R) that all the experimentally allowed ranges of mixing angles, at 2σ error levels, can be covered in this pattern except for inverted hierarchy type where θ_y is restricted to be greater than 48°. This restriction on θ_y distinguishes the inverted hierarchy type in this model. However, no obvious clear correlation can be revealed in these plots. The plots (d-L, e-L) show that the phases are not constrained at all. However, in the case of degenerate and inverted hierarchy, there is a strong linear correlation of δ versus ρ and σ, whereas this correlation almost disappears in the normal hierarchy case. There is also (plot f-R) a linear correlation between the Majorana phases which is clearly apparent in the normal and inverted hierarchy types while a bit blurred in the degenerate case.

The correlations (J, δ) and (J, θ_z) have each a specific geometrical shape which is hierarchy-type independent as it is clear from Fig. 1 (plots: f-L, e-R). This behavior can be understood from the formula of J given in Eq. (18). In fact, the correlation (J, δ) can be seen as the superposition of many sinusoidal graphs in δ whose "positive" amplitudes are determined by the acceptable mixing angles, whereas the (J, θ_z) correlation is formed by the superposition of straight lines in $s_z \sim z$, for small z, whose slopes can be positive or negative depending on the sign of s_δ.

The correlations of $\langle m\rangle_{ee}$ against $(\theta_x, \theta_y, \delta, \rho, \sigma, J)$, as inferred from plot (d-R) of Fig. 1 and from the left panel of Fig. 2 (plots: a-L $\rightarrow$ e-L), show that a lower bound for $\langle m\rangle_{ee}$ would generally constrain the allowed parameter space. There is also a general tendency of decreasing $\langle m\rangle_{ee}$ with increasing θ_y in the case of inverted hierarchy (plot aI-L). Another important point concerning $\langle m\rangle_{ee}$ is that it can attain the zero limit in the normal hierarchy case, as is evident from the graphs or explicitly from the corresponding covered range in Table I. This limit essentially corresponds to the case of vanishing $M_{\nu 11}$ [Eq. (17)] which, when combined with vanishing C_{33} condition, implies vanishing $M_{\nu 12}$. This means that in the limit of zero m_{ee} we recover a corresponding two-zero texture. It should be noted that this pattern of two-zero-entries texture is equivalent to the model of vanishing two minors C_{33} and C_{32} [11]. For the correlation of m_2/m_3 versus θ_y (plot f-L), we see that if the angle θ_y is in the first octant then m_2 is less than m_3.

The right panel of Fig. 2 does not show clear correlation for θ_y against (ρ, σ) (plots: a-R, b-R), whereas it indicates a correlation of J versus (ρ, σ) (plots: c-R, d-R) which is a direct consequence of the correlations of δ against (ρ, σ). The two correlations concerning the LNM (plots: e-R, f-R)

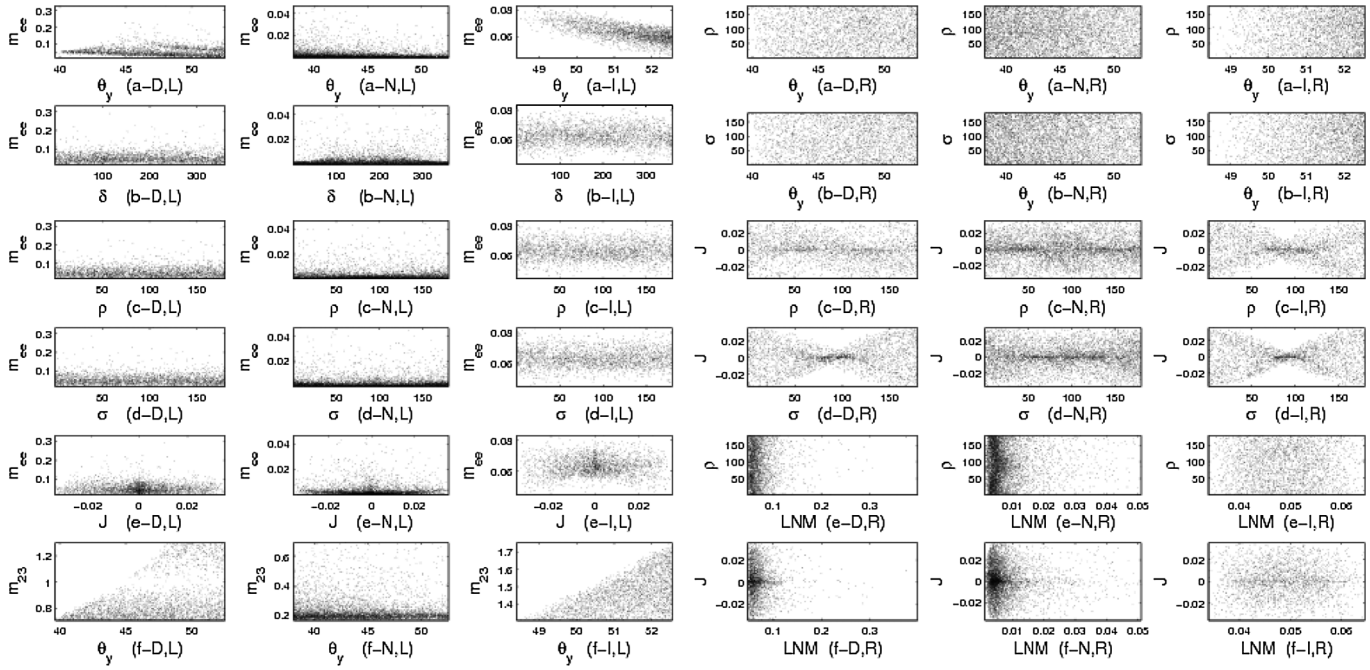

FIG. 2. Pattern $\mathbf{C}_{33}$: The left panel presents correlations of m_{ee} against θ_y, δ, ρ, σ, and J. It also shows the correlation between m_2/m_3 and θ_y. The right panel shows correlations of (ρ, σ) against θ_y and J and those of the lowest neutrino mass (LNM) versus ρ and J.

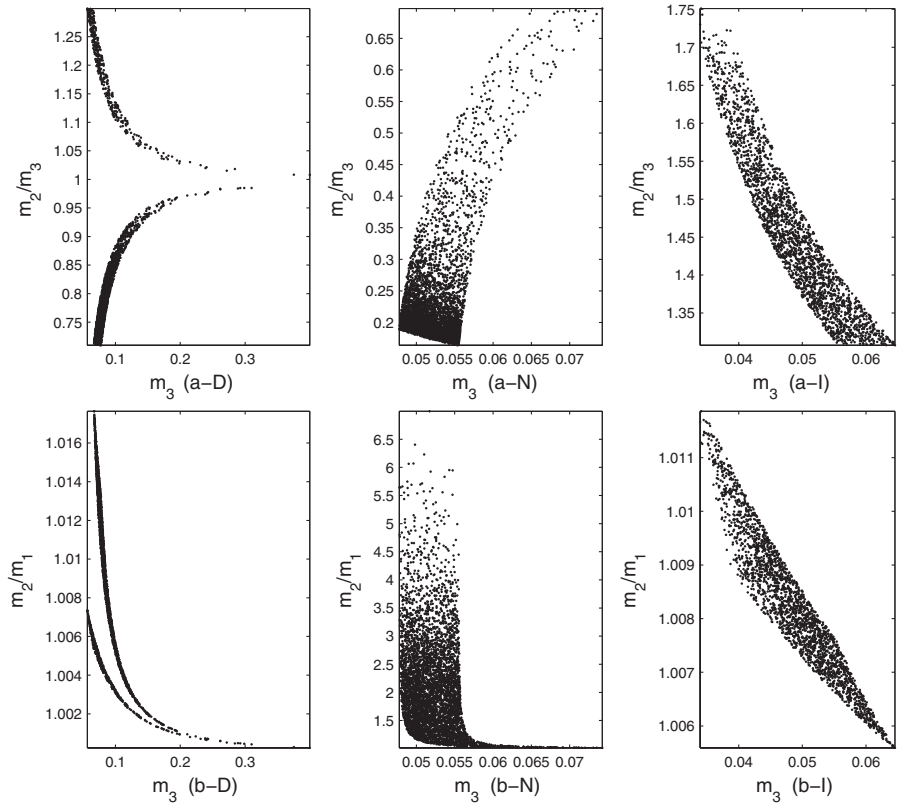

FIG. 3. Pattern $\mathbf{C}_{33}$: correlations of mass ratios $\frac{m_2}{m_3}$ and $\frac{m_2}{m_1}$ against m_3.

generally reveal that as the LNM increases the parameter space becomes more restricted, and this seems to be a general trend with increasing neutrino mass scale.

For the mass spectrum, as illustrated in Fig. 3, we see that the normal and inverted hierarchy are of moderate type in that the ratios do not reach extremely high, nor low, values. The degenerate and inverted hierarchy types are characterized by nearly equal values of m_1 and m_2. We also see that if m_3 is large enough then only the degenerate case with $m_1 \sim m_2$ can be compatible with data. We checked that there was no singular texture which can accommodate the data, although the limit $\theta_z = 0$ can be reached. This can be seen from the coverable ranges of masses m_1 and m_3 in Table I. This table also shows that no inverted hierarchy type of this pattern could be obtained at the 1σ precision level.

B. Pattern of vanishing minor C_{22}; $M_{\nu 11}M_{\nu 33} - M_{\nu 13}M_{\nu 13} = 0$

In this model, the relevant expressions for A_1, A_2, and A_3 are

$$\begin{aligned} A_1 &= (s_x c_y + s_z c_x s_y e^{-i\delta})^2, \\ A_2 &= (c_x c_y - s_z s_x s_y e^{-i\delta})^2, \\ A_3 &= c_z^2 s_y^2 e^{-2i\delta}. \end{aligned} \tag{35}$$

We get

$$\frac{m_1}{m_3} \approx \frac{s_x^2 s_{2\rho-2\sigma}}{t_y^2 s_{2\sigma-2\delta}} + O(s_z) \tag{36}$$

$$\frac{m_2}{m_3} \approx \frac{c_x^2 s_{2\rho-2\sigma}}{t_y^2 s_{2\delta-2\rho}} + O(s_z). \tag{37}$$

Again, there is no singular such texture which can accommodate the data. As for the plots, and since this pattern is related by T_2 symmetry to the pattern C_{33}, they can be deduced from those of the latter pattern but after changing θ_y and δ accordingly.

C. Pattern of vanishing minor C_{31}; $M_{\nu 12}M_{\nu 23} - M_{\nu 13}M_{\nu 22} = 0$

The relevant expressions for A_1, A_2, and A_3 for this model are

$$\begin{aligned} A_1 &= c_z c_x (s_y s_x - s_z c_x c_y e^{-i\delta}) e^{-i\delta} \\ A_2 &= -c_z s_x (s_y c_x + s_z s_x c_y e^{-i\delta}) e^{-i\delta}, \\ A_3 &= s_z c_z c_y e^{-2i\delta}. \end{aligned} \tag{38}$$

We obtain

$$\frac{m_1}{m_3} \approx \frac{t_y c_x s_x s_{2\rho-2\sigma}}{s_{2\sigma-\delta} s_z} + O(s_z) \tag{39}$$

$$\frac{m_2}{m_3} \approx \frac{t_y c_x s_x s_{2\sigma-2\rho}}{s_{\delta-2\rho} s_z} + O(s_z). \tag{40}$$

We have also

$$R_\nu = \frac{c_{2\sigma} c_{2\sigma+2\delta} - c_{2\rho} c_{2\rho-2\delta}}{c_\delta^2 - c_{2\sigma} c_{2\sigma-2\delta}} + O(s_z). \tag{41}$$

We plot the correlations in Figs. 4–6 with the same conventions as in the case of the C_{33} pattern. Compared to the latter case, we see that the mixing angles $(\theta_x, \theta_y, \theta_z)$ can cover all their allowable regions (Fig. 4, plots: a-L → c-L, a-R → c-R) and in all hierarchy types. The linear correlations of δ versus ρ and σ disappear in the inverted case, whereas they are replaced by Lissajous-like patterns in the degenerate case (Fig. 4, plots: d-L, e-L). However, there is an acute linear correlation between ρ and σ (Fig. 4, plot: f-R) in the degenerate and normal cases. The special ''sinusoidal'' and ''isosceles'' shapes of J versus δ and θ_z remain (Fig. 4, plots: f-L, e-R), but we note that in the normal case the sinusoidal shape is concentrated for δ in the first and fourth quarters, which would single out a disallowed region for δ ranging from 123° to 242° approximately. Again no clear correlation involves m_{ee} (Fig. 4 plot d-R, Fig. 5 plots: a-L → e-L). However, setting a lower bound on this parameter would constrain the parameter space only in the degenerate case. Apart from the usual correlations of J versus ρ and σ (Fig. 5 plots: c-R, d-R), originating from the correlation of δ with ρ and σ, the other plots doe not show clear correlations. We see from Table I that the limit $m_{ee} = 0$ is not attainable in this pattern.

For the mass spectrum, the plot b-I in Fig. 6 tells us that the experimental data can be accommodated in the inverted hierarchy type only when the two masses m_1 and m_2 are approximately equal. However, the mass ratio parameter m_2/m_3 (plot a-I) indicates a strong hierarchy. This is to be contrasted with the normal type hierarchy case (plots a-N and b-N) where the hierarchy is mild and the mass ratios are of order $O(1)$. We see also that in contrast to the pattern C_{33}, the limit $m_3 = 0$ can be reached. In fact, there is a noninvertible such texture which can accommodate the current data, and this happens only when $\theta_z = 0$ leading to $m_3 = 0$.

D. Pattern of vanishing minor C_{32}; $M_{\nu 11}M_{\nu 23} - M_{\nu 21}M_{\nu 13} = 0$

The relevant expressions for A_1, A_2, and A_3 for this model are

$$\begin{aligned} A_1 &= -(s_z c_x c_y e^{-i\delta} - s_x s_y)(s_x c_y + s_z c_x s_y e^{-i\delta}), \\ A_2 &= -(c_y s_z s_x e^{-i\delta} + s_y c_x)(s_y s_z s_x e^{-i\delta} - c_y c_x), \\ A_3 &= -c_z^2 s_y c_y e^{-2i\delta}. \end{aligned} \tag{42}$$

We get

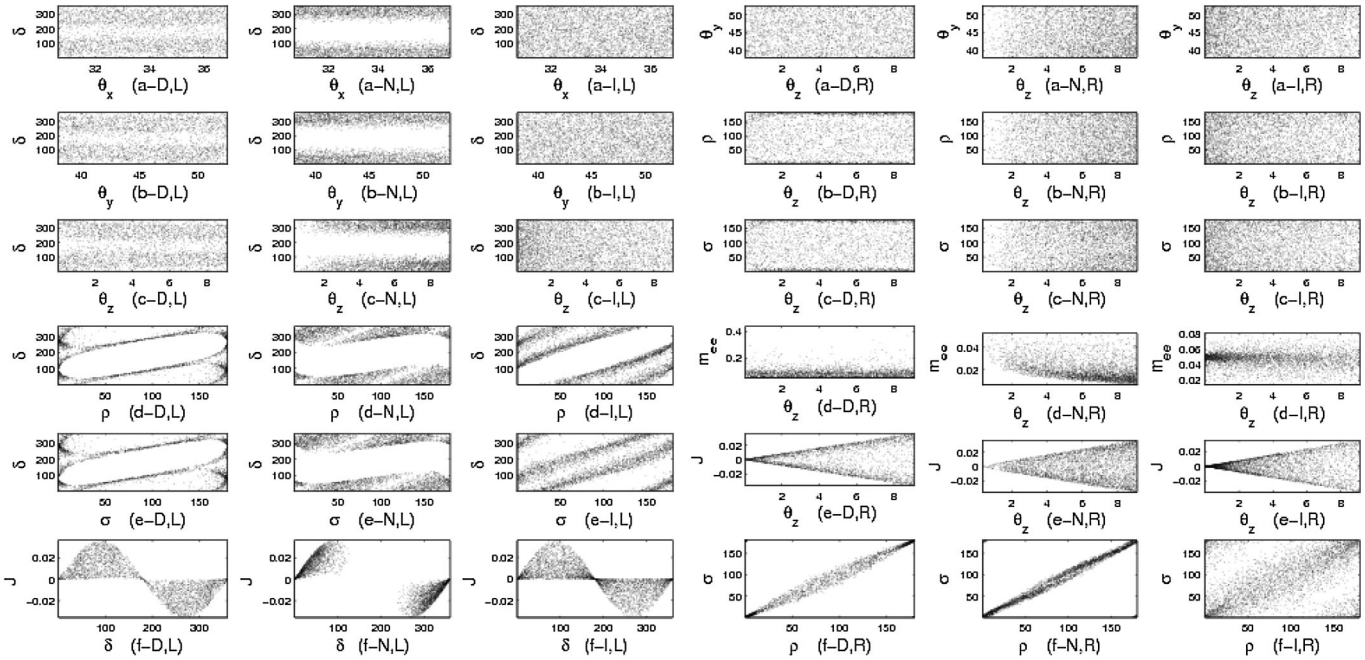

FIG. 4. Pattern $\mathbf{C}_{31}$: The left panel presents correlations of δ against mixing angles, CP phases, and J, while the right panel shows the correlations of θ_z against θ_y, ρ, σ, m_{ee}, and J, and also the correlation of ρ versus σ.

$$\frac{m_1}{m_3} \approx \frac{s_x^2 s_{2\sigma-2\rho}}{s_{2\sigma-2\delta}} + O(s_z) \tag{43}$$

$$\frac{m_2}{m_3} \approx \frac{c_x^2 s_{2\rho-2\sigma}}{s_{2\rho-2\delta}} + O(s_z). \tag{44}$$

Upon spanning the parameter space, we checked that no inverted hierarchy could accommodate the data. We produce the correlation plots in Figs. 7–9. We see that the mixing angles and phase angles can cover their experimentally allowed regions. Linear correlations between δ and (ρ, σ) are apparent in the degenerate case, whereas the

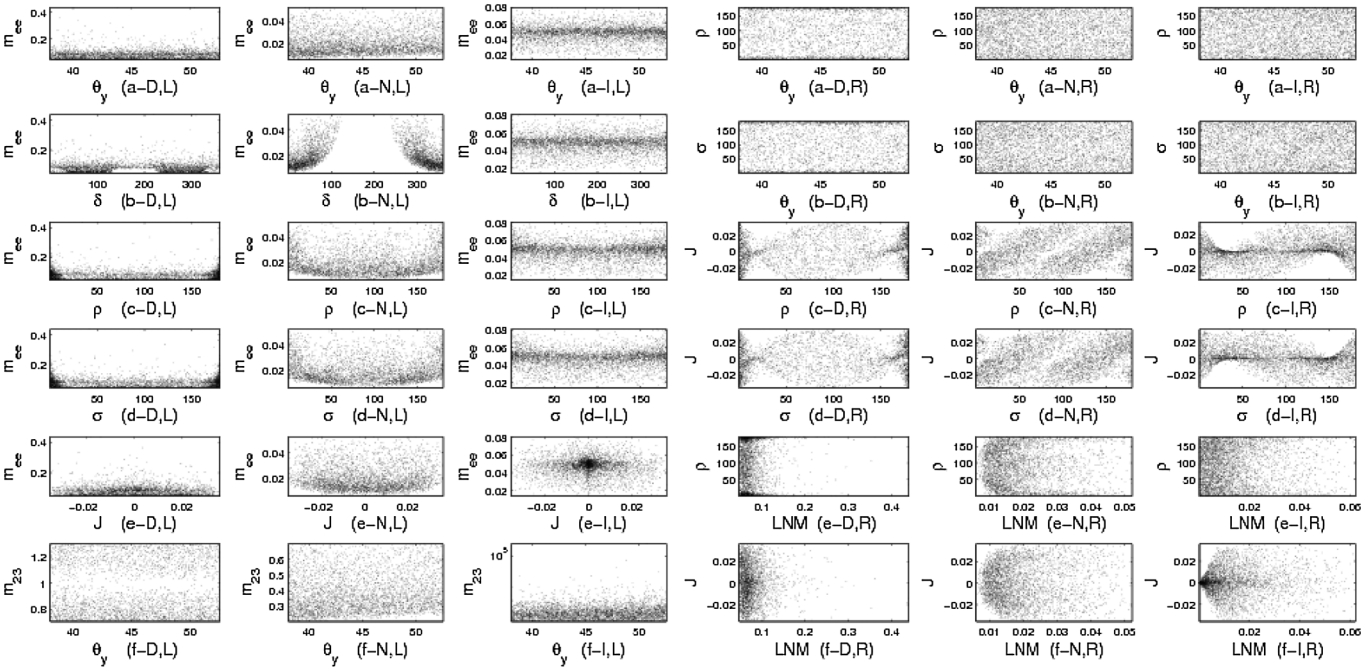

FIG. 5. Pattern $\mathbf{C}_{31}$: The left panel presents correlations of m_{ee} against θ_y, δ, ρ, σ, and J. It also shows the correlation between m_2/m_3 and θ_y. The right panel shows correlations of (ρ, σ) against θ_y and J and those of the lowest neutrino mass (LNM) versus ρ and J.

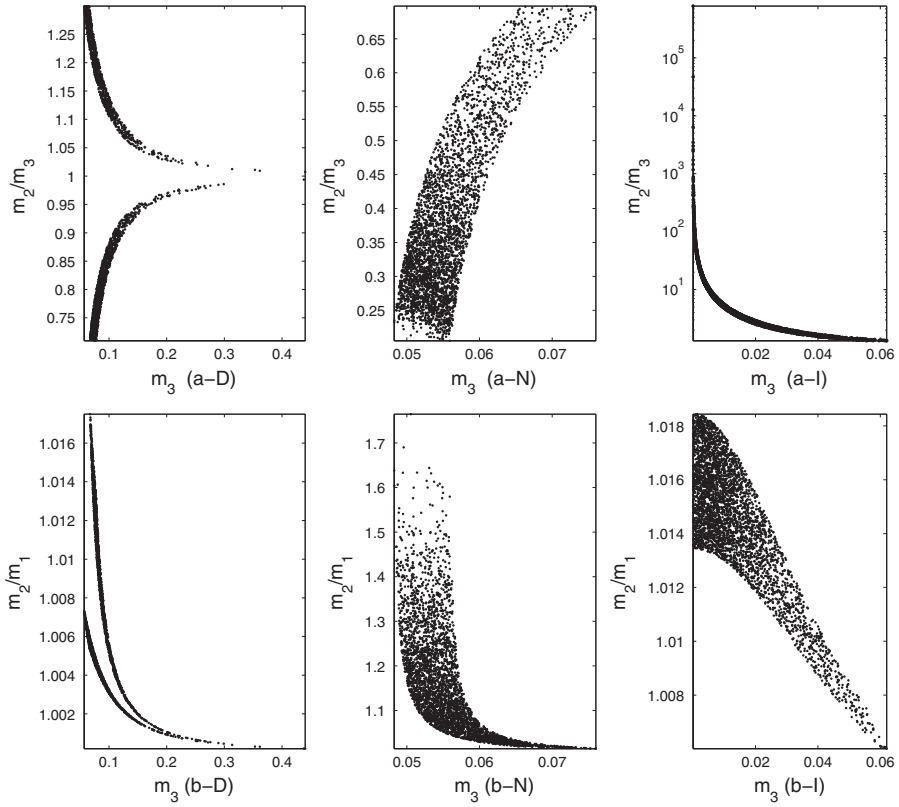

FIG. 6. Pattern $\mathbf{C}_{31}$: correlations of mass ratios $\frac{m_2}{m_3}$ and $\frac{m_2}{m_1}$ against m_3.

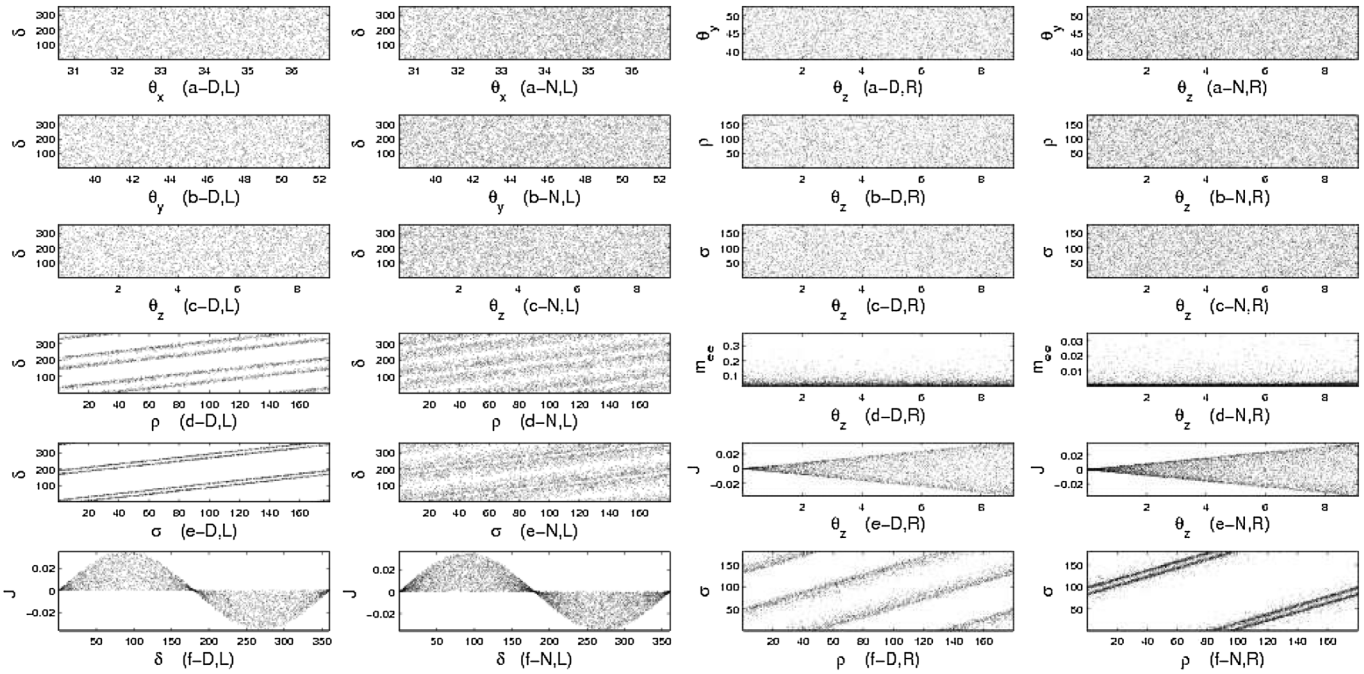

FIG. 7. Pattern $\mathbf{C}_{32}$: The left panel presents correlations of δ against mixing angles, *CP* phases, and J, while the right panel shows the correlations of θ_z against θ_y, ρ, σ, m_{ee}, and J, and also the correlation of ρ versus σ.

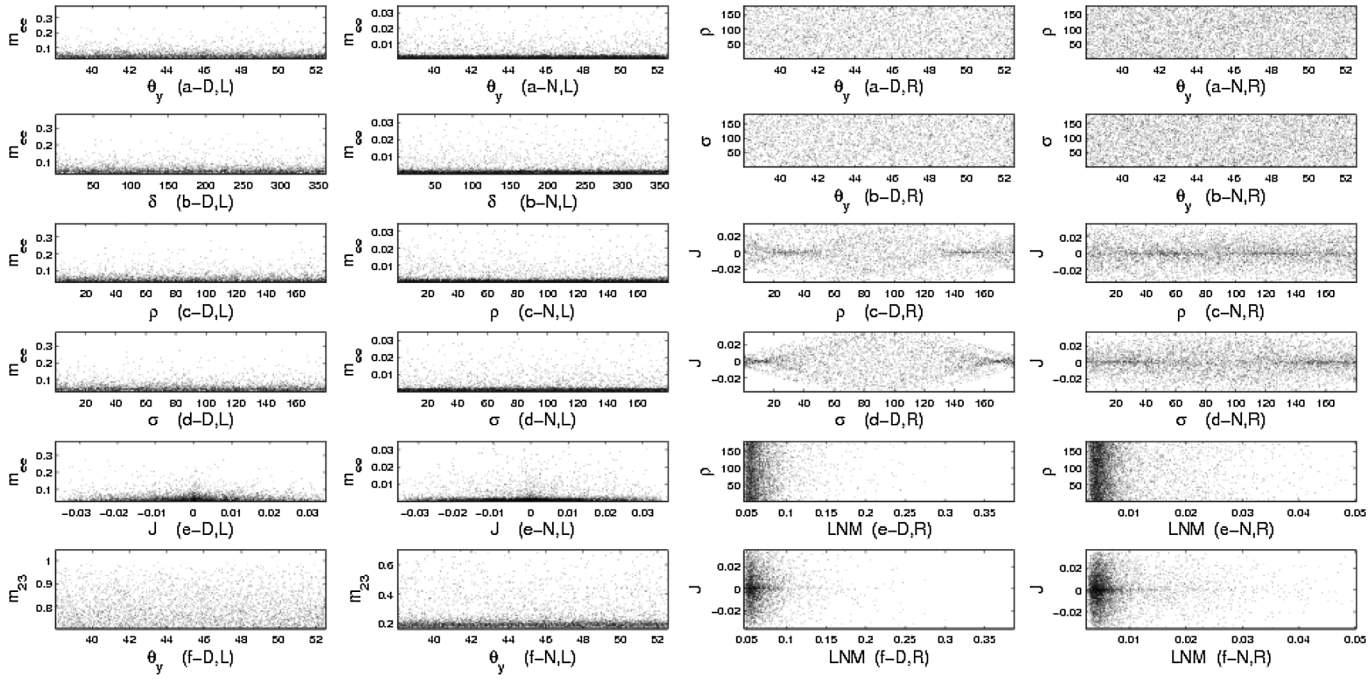

FIG. 8. Pattern $\mathbf{C}_{32}$: The left panel presents correlations of m_{ee} against θ_y, δ, ρ, σ, and J. It also shows the correlation between m_2/m_3 and θ_y. The right panel shows correlations of (ρ, σ) against θ_y and J and those of the lowest neutrino mass (LNM) versus ρ and J.

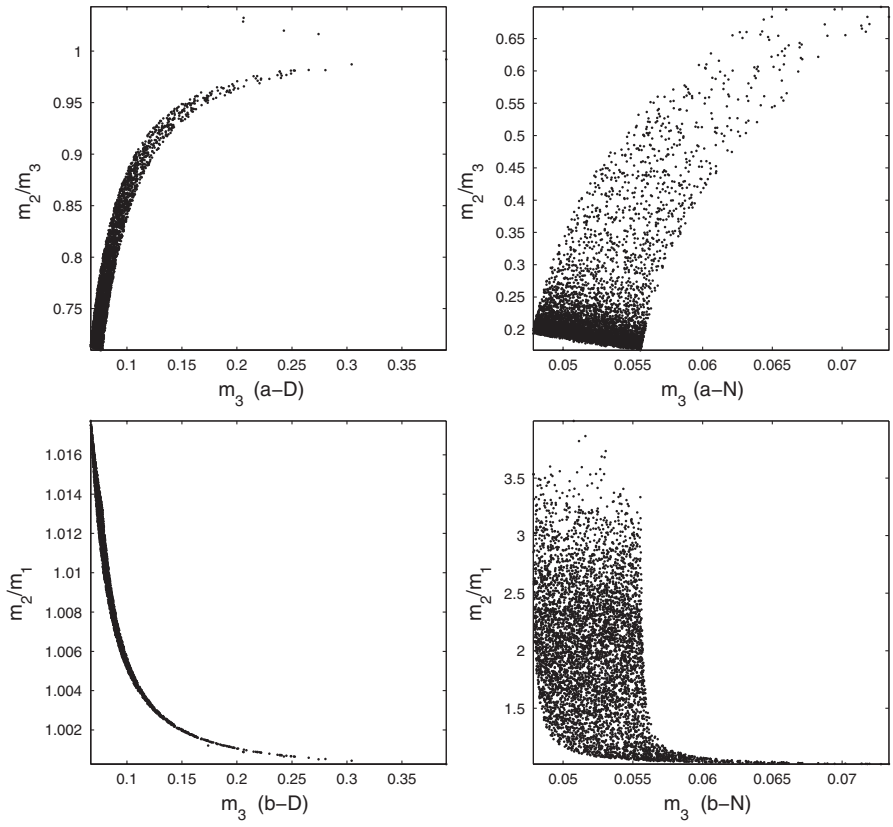

FIG. 9. Pattern $\mathbf{C}_{32}$: correlations of mass ratios $\frac{m_2}{m_3}$ and $\frac{m_2}{m_1}$ against m_3.

linear correlation of ρ versus σ is also apparent in the normal case. The sinusoidal and isosceles shapes of the (J, δ) and (J, θ_z) correlations are uniformly covered. Again, the correlations of m_{ee} show that a lower bound on this parameter restricts enormously the parameter space. These correlation plots, or alternatively Table II, show that the limit $m_{ee} = 0$ can be met in the normal hierarchy case. Moreover, the pattern in this limit is a two-zero entries texture with $M_{\nu 11} = M_{\nu 12} = 0$ or $M_{\nu 11} = M_{\nu 13} = 0$. The equivalent models for two vanishing minors texture [11] are the T_1-symmetry related models: (vanishing C_{33} and C_{32}) and (vanishing C_{22} and C_{32}). Again, no clear correlation between (m_{23}, θ_y), nor between θ_y and (ρ, σ). One can find a mild correlation of J versus ρ and σ, originating from the linear correlation of δ with (ρ, σ), especially in the degenerate case. As to the LNM correlations, the trend is to favor a lower value for this parameter in that increasing its value would cut short the parameter space. Numerically, the lower bounds on $\theta_z = 0$ reached very tiny values in this pattern (look at Table II).

For the mass spectrum, the normal hierarchy is not acute, in that the ratio m_2/m_3 has a lower bound of order 0.2 (plot a-N in Fig. 9). We note also that no mass can approach too closely to zero. We see this in the normal hierarchy either by looking at (Fig. 9, plot b-N) and noting that $\frac{m_2}{m_1}$ is not reaching very large values corresponding to very minute m_1, or by checking the coverable mass regions in Table II.

There is no noninvertible such texture which can accommodate the current data.

E. Pattern of vanishing minor C_{21}; $M_{\nu 21}M_{\nu 33} - M_{\nu 31}M_{\nu 23} = 0$

The relevant expressions for A_1, A_2, and A_3 for this model are

$$\begin{aligned} A_1 &= c_z c_x (c_y s_x + s_z c_x s_y e^{-i\delta}) e^{-i\delta} \\ A_2 &= -c_z s_x (c_y c_x - s_z s_x s_y e^{-i\delta}) e^{-i\delta}, \\ A_3 &= s_z c_z c_y e^{-2i\delta}. \end{aligned} \tag{45}$$

We get

$$\frac{m_1}{m_3} \approx \frac{c_x s_x s_{2\sigma-2\rho}}{s_{2\sigma-\delta} s_z t_y} + O(1) \tag{46}$$

$$\frac{m_2}{m_3} \approx \frac{c_x s_x s_{2\sigma-2\rho}}{s_{\rho-\delta} s_z t_y} + O(1) \tag{47}$$

with

$$R_\nu = \frac{c_{2\rho} c_{2\rho-2\delta} - c_{2\sigma} c_{2\sigma-2\delta}}{c_{2\sigma} c_{2\sigma-2\delta} - c_\delta^2} + O(s_z). \tag{48}$$

The phenomenological analysis of this pattern can be deduced from that of C_{31} which is equivalent under the symmetry T_1.

Also, and as in the pattern C_{31}, there is a noninvertible such texture which can accommodate the current data, and this happens only when $\theta_z = 0$ leading to $m_3 = 0$.

F. Pattern of vanishing minor C_{11}; $M_{\nu 22}M_{\nu 33} - M_{\nu 32}M_{\nu 23} = 0$

The quantities A_1, A_2, and A_3, corresponding to the model, are

$$A_1 = c_z^2 s_x^2 e^{-2i\delta}, \qquad A_2 = c_z^2 s_x^2 e^{-2i\delta}, \qquad A_3 = s_z^2 e^{-2i\delta}. \tag{49}$$

The analytical expressions for all relevant computed parameters are simple and independent of δ. The mass ratios take the forms

$$\frac{m_1}{m_3} = \frac{c_x^2 s_{2\rho-2\sigma}}{t_z^2 s_{2\sigma}} \tag{50}$$

$$\frac{m_2}{m_3} = \frac{s_x^2 s_{2\sigma-2\rho}}{t_z^2 s_{2\rho}}. \tag{51}$$

Fixing the $\Delta m^2_{\rm sol}$ at its central value [Eq. (20)], one can compute m_3:

$$m_3 = \frac{\sqrt{\Delta m^2_{\rm sol}}\, t_z^2}{|s_{2\sigma-2\rho}| \sqrt{|(\frac{s_x^4}{s_{2\rho}^2} - \frac{c_x^4}{s_{2\sigma}^2})|}}. \tag{52}$$

We thus can get the corresponding expression of $\Delta m^2_{\rm atm}$ as

$$\Delta m^2_{\rm atm} = m_3^2 \left| 1 - \frac{s_x^4 s_{2\sigma-2\rho}^2}{t_z^4 s_{2\rho}^2} \right|. \tag{53}$$

The nonoscillation parameters $\langle m \rangle_e$, $\langle m \rangle_{ee}$, and Σ are given as

$$\begin{aligned} \langle m \rangle_e &= m_3 \sqrt{\left[\frac{c_z^2}{t_z^4} s_{2\sigma-2\rho}^2 \left(\frac{c_x^6}{s_{2\sigma}^2} + \frac{s_x^6}{s_{2\rho}^2} \right) + s_z^2 \right]}, \\ \langle m \rangle_{ee} &= m_3 \left| \frac{c_x^2}{t_z^2} \frac{s_{2\rho-2\sigma}}{s_{2\sigma}} c_x^2 c_z^2 e^{2i\rho} + \frac{s_x^2}{t_z^2} \frac{s_{2\sigma-2\rho}}{s_{2\rho}} s_x^2 c_z^2 e^{2i\sigma} + s_z^2 \right|, \\ \Sigma &= m_3 \left| \frac{c_x^2}{t_z^2} \frac{s_{2\rho-2\sigma}}{s_{2\sigma}} + \frac{s_x^2}{t_z^2} \frac{s_{2\sigma-2\rho}}{s_{2\rho}} + 1 \right|, \end{aligned} \tag{54}$$

where m_3 is given in Eq. (52). Finally the parameter R_ν has the form

$$R_\nu = \frac{s_{2\sigma-2\rho}^2 (\frac{s_x^4}{s_{2\rho}^2} - \frac{c_x^4}{s_{2\sigma}^2})}{1 - \frac{s_x^4 s_{2\sigma-2\rho}^2}{t_z^4 s_{2\rho}^2}}. \tag{55}$$

This pattern shows only inverted-type hierarchy, and the corresponding plots are shown in Figs. 10 and 11. We see in Fig. 10 that the mixing angles $(\theta_x, \theta_y, \theta_z)$ and the Dirac phase angle δ cover all their allowable regions (plots: a-L $\rightarrow$ c-L, g-L $\rightarrow$ i-L). However, the region around $\rho = \frac{\pi}{2}$ or $\sigma = \frac{\pi}{2}$ tends to be excluded (look also at the two plots:

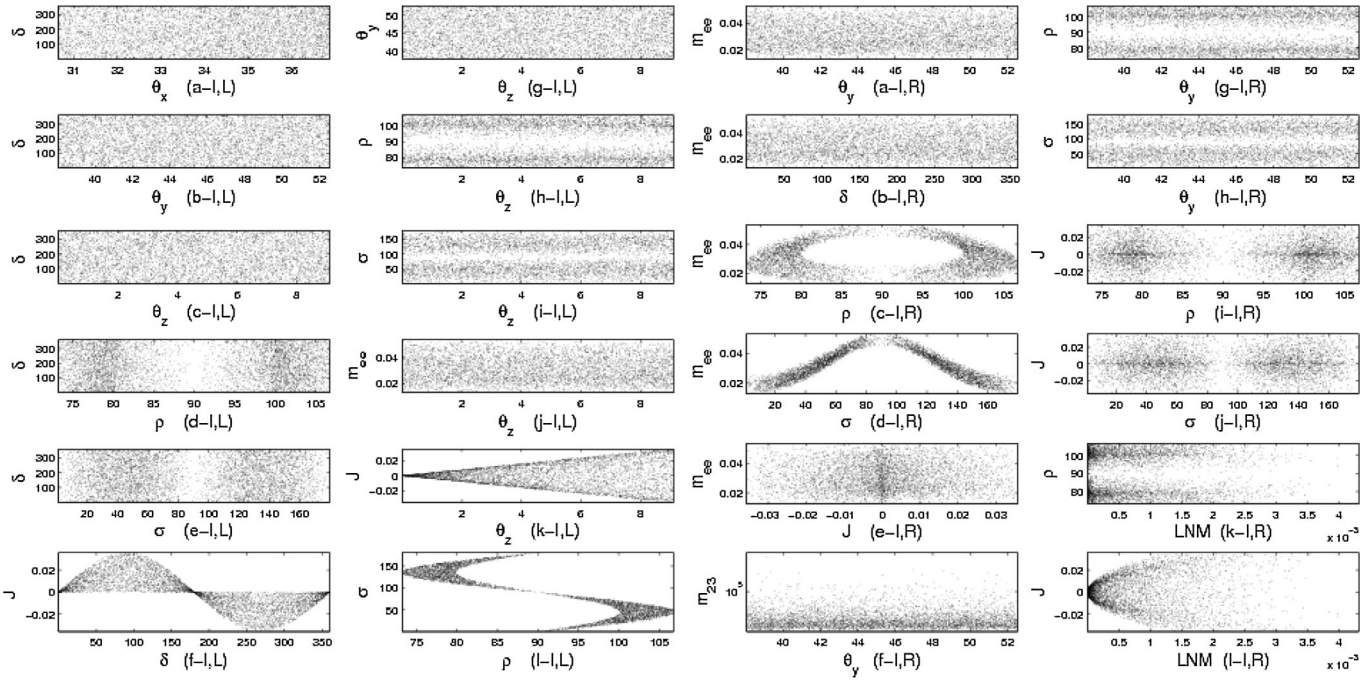

FIG. 10. Pattern $\mathbf{C}_{11}$: The left panel presents, in the first column, correlations of δ against mixing angles, *CP* phases, and J. It also shows, in the second column, correlations of θ_z against θ_y, ρ, σ, m_{ee}, and J, and the correlation of ρ versus σ. The right panel shows, in the third column, correlations of m_{ee} against θ_y, δ, ρ, σ, and J, and also the correlation between m_2/m_3 and θ_y. It presents in the last column correlations of (ρ, σ) against θ_y and J and those of the lowest neutrino mass (LNM) versus ρ and J.

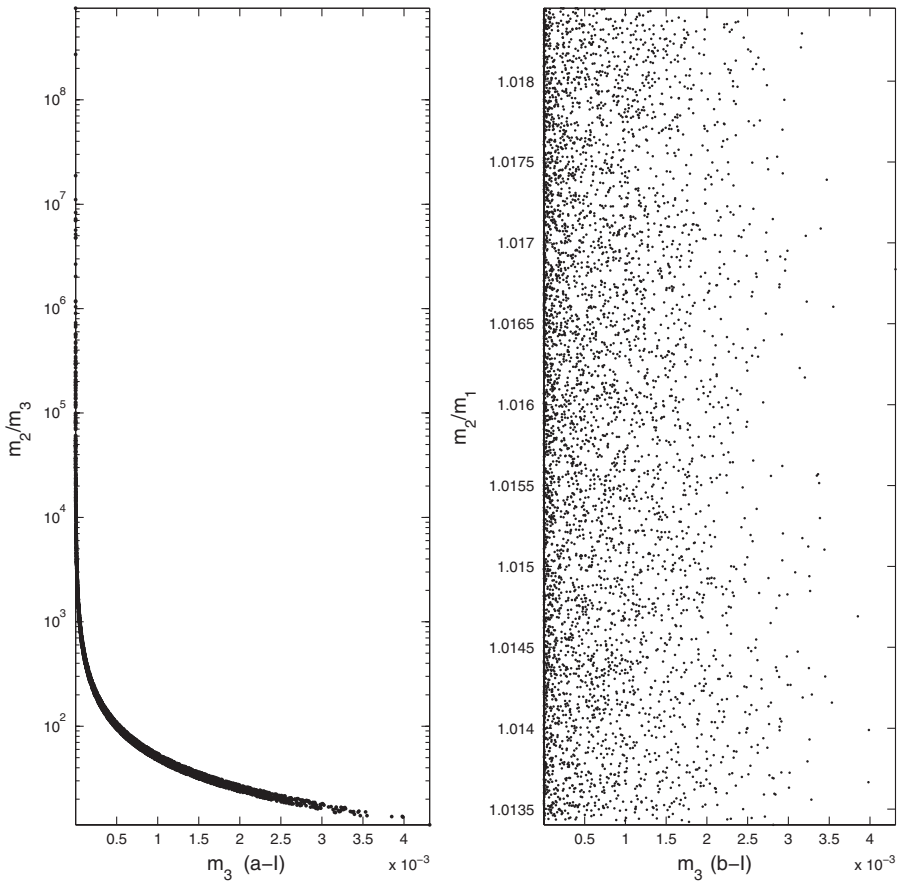

FIG. 11. Pattern $\mathbf{C}_{11}$: correlations of mass ratios $\frac{m_2}{m_3}$ and $\frac{m_2}{m_1}$ against m_3.

g-R, h-R), in accordance with the analytic formulas, say [Eq. (51)] where these limits would equate the denominators to zero. Moreover, the analytic expressions [e.g. Eq. (52)] would exclude the region of $\rho - \sigma$ equal to a multiple of $\frac{\pi}{2}$. Furthermore, setting the ratio m_2/m_1 to be larger than 1 and taking into account that t_x is less than one, for the experimentally accepted θ_x, would force the ratio $|\frac{s_{2\sigma}}{s_{2\rho}}|$ to be larger than 1. This, with the fact that the difference $\rho - \sigma$ should not vanish, would put a lower bound on σ, as one can see in Table II. In this Table we see also a restricted region for ρ due to the $\Delta^2_{\rm atm}$ formula barring small values of ρ. Plots (d-L, e-L) show no strong correlation between (δ, ρ) nor between (δ, σ), whence no clear correlation between J versus ρ, or between J versus σ (plots: i-R, j-R). There is a strong sinusoidal correlation between σ against ρ (plot: l-L) showing that σ being in the first quarter forces ρ to be in the second quarter, and vice versa. The correlations of m_{ee} have a clear shape only versus ρ and σ. These shapes can be deduced from the analytical formula [Eq. (54)]. The LNM correlation with ρ (plot k-R) again excludes the region around $\rho = \frac{\pi}{2}$, whereas its correlation with J favors, for very small values of LNM, a vanishing J with no CP violation effects.

The mass spectrum in Fig. 11 shows a quite strong inverted hierarchy (plot a-I) with $m_1 \sim m_2$ (plot b-I), and that we can approach the limit $m_3 = 0$. In fact, there is a viable singular such texture when $\theta_z = 0$ and $m_3 = 0$.

From the two tables we see that the value $m_3 = 0$ is attained in the inverted hierarchy for the patterns (C_{11}) and (C_{31}, C_{21}), the latter two being related by T_1 symmetry.

V. SINGULAR MODELS

The viable singular models obtained in cases $\mathbf{C}_{31} \equiv C_{21}$ and $\mathbf{C}_{11}$ are found only for vanishing m_3, albeit with zero θ_z. A vanishing θ_z is still consistent with experimental data as shown in Eq. (21). These models can accommodate the experimental data for the mixing angles for any choice of the phase angles. It is interesting to notice that the models $\mathbf{C}_{31} \equiv C_{21}$ and $\mathbf{C}_{11}$ have quite distinct mass spectra but, in the singular limit ($m_3 = 0$ and $\theta_z = 0$), the models become exactly identical leaving no room for any kind of distinguishability.

In fact, this model is identical to the singular model studied in [11] for the vanishing two-minors textures. For the sake of completeness we restate here the expressions for the mass parameters,

$$m_1 = \sqrt{\Delta m^2_{\rm atm} - \Delta m^2_{\rm sol}}, \qquad m_2 = \sqrt{\Delta m^2_{\rm atm}}, \qquad \langle m \rangle_e = \sqrt{m_1^2 c_x^2 + m_2^2 s_x^2} \tag{56}$$

$$\langle m \rangle_{ee} = \sqrt{|m_1^2 c_x^4 + m_2^2 s_x^4 + 2 m_1 m_2 c_x^2 s_x^2 c_{2\rho - 2\sigma}|}, \tag{57}$$

and the mass matrix elements,

$$\begin{aligned}
M_{\nu 11} &= (m_1 c_x^2 e^{2i\rho} + m_2 s_x^2 e^{2i\sigma}),\\
M_{\nu 12} &= s_x c_x c_y e^{-i\delta}(-m_1 e^{2i\rho} + m_2 e^{2i\sigma}),\\
M_{\nu 13} &= s_x c_x s_y e^{-i\delta}(m_1 e^{2i\rho} - m_2 e^{2i\sigma}),\\
M_{\nu 22} &= c_y^2 e^{-2i\delta}(m_1 s_x^2 e^{2i\rho} + m_2 c_x^2 e^{2i\sigma}),\\
M_{\nu 23} &= -c_y s_y e^{-2i\delta}(m_1 s_x^2 e^{2i\rho} + m_2 c_x^2 e^{2i\sigma}),\\
M_{\nu 33} &= s_y^2 e^{-2i\delta}(m_1 s_x^2 e^{2i\rho} + m_2 c_x^2 e^{2i\sigma}).
\end{aligned} \tag{58}$$

VI. SYMMETRY REALIZATION

All textures with one zero minor can be realized in a simple way in models based on seesaw mechanism with a flavor Abelian symmetry. As mentioned earlier, if the Dirac neutrino mass matrix M_D is diagonal then a zero in the right-handed Majorana mass matrix M_R leads to a zero minor in the effective neutrino mass matrix M_ν.

We need three right-handed neutrinos ν_{Rj}, three right-handed charged leptons l_{Rj}, and three left-handed lepton doublets $D_{Lj} = (\nu_{Lj}, l_{Lj})^T$, where j is the family index. Also we need the standard model (SM) Higgs, plus other scalar singlets. We follow [10] and assume a Z_8 underlying symmetry. For the sake of illustration, let us take the case of C_{33}. Under the action of Z_8, the leptons (the right singlets and the components of the left doublets) of the first, second, and third families are multiplied by $(1, -1, \omega = \exp(\frac{i\pi}{4}))$ respectively, while the SM Higgs remains invariant. This generates diagonal Dirac mass matrices for both charged leptons and neutrinos.

The bilinears $\nu_{Ri}\nu_{Rj}$, relevant for the Majorana neutrino mass matrix M_R, transform under Z_8 as

$$\begin{pmatrix} 1 & \omega^4 & \omega \\ \omega^4 & 1 & \omega^5 \\ \omega & \omega^5 & \omega^2 \end{pmatrix}. \tag{59}$$

The (1, 1) and (2, 2) matrix elements of M_R are Z_8 invariant, hence their corresponding mass terms are directly present in the Lagrangian. We require a Yukawa coupling to a real scalar singlet (χ_{12}) which changes sign under Z_8 to generate the (1, 2) matrix element in M_R, when acquiring a vev at the seesaw scale. The (2, 3) matrix element is equally generated by the Yukawa coupling to a complex scalar singlet (χ_{23}) with a multiplicative number ω^3 under Z_8, while the (1, 3) matrix element requires a Yukawa coupling to a complex scalar singlet (χ_{13}) which gets multiplied by ω^7 under Z_8. The resulting right-handed Majorna mass matrix can be cast in the form

$$M_R = \begin{pmatrix} \times & \times & \times \\ \times & \times & \times \\ \times & \times & 0 \end{pmatrix}, \tag{60}$$

which is of the required form.

For the other patterns, they can be generated in a similar way summarized in Table III.

TABLE III. The Z_8 symmetry realization for six patterns of single vanishing minors. The index 1_F indicates the lepton first family and so on. The χ_{kj} denotes a scalar singlet which produces the entry (k, j) of the right-handed Majorana mass matrix when acquiring vacuum expectation at the seesaw scale. The transformation properties, under the specified group, are listed below each family and needed scalar singlet for each model. ω denotes $\exp(\frac{i\pi}{4})$, while $i = \sqrt{-1}$.

Model	1_F	2_F	3_F	χ_{11}	χ_{12}	χ_{13}	χ_{22}	χ_{23}	χ_{33}
C_{33}	1	-1	ω	Absent	-1	ω^7	Absent	ω^2	Absent
C_{22}	1	ω	-1	Absent	ω^7	-1	Absent	ω^3	Absent
C_{13}	1	ω	-1	Absent	ω^7	Absent	ω^6	ω^3	Absent
C_{32}	1	ω	-1	Absent	ω^7	-1	ω^6	Absent	Absent
C_{12}	1	ω	-1	Absent	absent	-1	ω^6	ω^3	Absent
C_{11}	ω	-1	1	Absent	ω^3	ω^7	Absent	-1	Absent

The models C_{31}, C_{21}, and C_{11} in the limit of vanishing m_3 and θ_z together give a singular mass matrix M_ν. In fact, one symmetry realization of such a singular model was stated in [11].

VII. DISCUSSION AND CONCLUSIONS

We studied all the possible patterns of Majorana neutrino mass matrices with one vanishing minor. All six possible cases allow one to accommodate the current data without need to tune the input parameters. None of the patterns appears as a ''one-zero'' texture and, for the chosen acceptable parameter points, all the matrices are complex displaying CP violation effects.

Noninvertible mass matrices with one vanishing minor occur only in the cases (C_{31}, C_{21}, and C_{11}) with $\theta_z = 0$ leading to $m_3 = 0$. These latter three cases coincide in the limit ($\theta_z \to 0$) with the model of two vanishing minors in a singular M_ν which was studied in [11], making the distinction between them difficult.

The model C_{32} cannot produce inverted-type hierarchy, whereas the model C_{11} has only this type of hierarchy. For all six patterns, the mixing and phase angles cover their experimentally allowed regions. Exceptions here are the pattern C_{33} (the T_1-symmetry related pattern C_{22}) where θ_y is bound in the inverted hierarchy type to be larger than 48° (smaller than 42°), the pattern C_{31} (the T_1-symmetry related pattern C_{21}) in the normal hierarchy case where the Dirac angle δ lies outside the interval $[123°, 242°]$ (approximately inside the interval $[60°, 300°]$), and the pattern C_{11} where the phases ρ and σ tend to be far from $\pi/2$.

In all patterns, except C_{11}, there is a linear correlation in the inverted and degenerate cases between δ and ρ or σ, whence a sharp correlation of J against these two latter phases. Also, a linear correlation exists between ρ and σ in all cases even though it ceases to be linear in the pattern C_{11}.

The limit $\theta_z = 0$ can be attained in all patterns. In models (C_{31}, C_{21}, and C_{11}), this limit corresponds to the singular inverted-hierarchy model with $m_3 = 0$. As to the parameter m_{ee}, it can reach the value 0, for the case of normal hierarchy, in the patterns C_{33}, C_{22}, and C_{32}, whereas this zero limit cannot be achieved in the other patterns.

These features can help in distinguishing between the four independent models (let us take them as C_{33}, C_{31}, C_{32}, C_{11}). If the measured values of the mass ratios indicate an inverted hierarchy type then there are only two acceptable models, out of the three models C_{33}, C_{31}, C_{11} allowing for this type of hierarchy, depending on the intensity of this inverted hierarchy. If the intensity is strong ($m_2/m_3 > 10$) then the correct pattern would be either C_{31} or C_{11}. A subsequent measurement of the phase angles (ρ, σ) can exclude the pattern C_{11} if it lies outside the ''narrow'' dotted region in plot l-I, L in Fig. 10. Now, if the intensity is mild ($m_2/m_3 < 10$) then the choice would be between the patterns C_{31} or C_{33}. In this case, a measurement of θ_y smaller than 48° would exclude the C_{33} pattern, whereas, in case $\theta_y > 48°$, a measurement of the phase angles σ, δ helps to decide which pattern can accommodate the data by comparing, say, to the narrow bands of plot e-I, L in Fig. 1. Table IV summarizes these ''experimental signatures'' in the case of inverted hierarchy.

If the mass measurements give a normal type of hierarchy, then the accepted patterns would be (C_{32}, C_{33}, and C_{13}). One indication here is when δ lies inside $[123°, 242°]$ which would exclude C_{31}. The narrow band of the linear correlation between ρ and σ in plot f-N, R in Fig. 4 can help to exclude C_{31} when δ lies outside the above interval. However, this measurement of ρ and σ can not distinguish between C_{32} and C_{33} (look at the similar plots of f-N, R in Figs. 1 and 7), and it would be difficult to distinguish between these two patterns. For the degenerate

TABLE IV. The inverted-hierarchy ''experimental'' signatures distinguishing the different patterns.

Intensity	Mild	Strong
Acceptable patterns	C_{33} and C_{13}	C_{11} and C_{13}
Signature	$\theta_y < 48° \Rightarrow C_{13}$	
Decisive phase angles	δ, σ	ρ, σ

type, the possible patterns would also be C_{32}, C_{33}, and C_{13}. Although we do not have a ''signature'' coming from the δ alone here, however the knowledge of all the phase angles together can distinguish between the patterns. This comes because the narrow ''bands'' corresponding to the linear correlations of (ρ, σ) are different in plots f-D, R of Fig. 4 and Fig. 7 which would help to exclude the cases C_{31} and C_{32}. Also, the different ''band'' structures of the linear correlations (δ, σ) in plots e-D, L of Fig. 1 and 7 would help to distinguish between the patterns C_{33} and C_{32}.

Finally, all the models can be realized in the framework of flavor Abelian discrete symmetry, with at most three additional SM-singlet scalar fields transforming appropriately, implemented in seesaw schemes.

ACKNOWLEDGMENTS

Both authors would like to thank A. Smirnov and S. Petcov for useful discussions. Part of this work was done within the associate schemes of ICTP and TWAS.

[1] Y. Fukuda *et al.*, Phys. Lett. B **436**, 33 (1998); Phys. Rev. Lett. **81**, 1562 (1998). For a review, see C. K. Jung, C. McGrew, T. Kajita, and T. Mann, Annu. Rev. Nucl. Part. Sci. **51**, 451 (2001).
[2] Q. R. Ahmad *et al.* (SNO Collaboration), Phys. Rev. Lett. **89**, 011301 (2002); **89**, 011302 (2002).
[3] K. Eguchi *et al.* (KamLAND Collaboration), Phys. Rev. Lett. **90**, 021802 (2003).
[4] M. H. Ahn *et al.* (K2K Collaboration), Phys. Rev. Lett. **90**, 041801 (2003).
[5] M. Apollonio *et al.* (CHOOZ Collaboration), Phys. Lett. B **420**, 397 (1998); F. Boehm *et al.* (Palo Verde Collaboration), Phys. Rev. Lett. **84**, 3764 (2000).
[6] P. H. Frampton, S. L. Glashow, and D. Marfatia, Phys. Lett. B **536**, 79 (2002).
[7] Z. Z. Xing, Phys. Lett. B **530**, 159 (2002).
[8] Z. Z. Xing, Phys. Rev. D **69**, 013006 (2004).
[9] W. Grimus, A. S. Joshipura, L. Lavoura, and M. Tanimoto, Eur. Phys. J. C **36**, 227 (2004).
[10] L. Lavoura, Phys. Lett. B **609**, 317 (2005).
[11] E. I. Lashin and N. Chamoun, Phys. Rev. D **78**, 073002 (2008).
[12] H. A. Alhendi, E. I. Lashin, and A. A. Mudlej, Phys. Rev. D **77**, 013009 (2008).
[13] S. Dev, S. Kumar, S. erma, and S. Gupta, Phys. Rev. D **76**, 013002 (2007).
[14] C. Jarlskog, Phys. Rev. Lett. **55**, 1039 (1985); Z. Phys. C **29**, 491 (1985); Phys. Rev. D **35**, 1685 (1987).
[15] G. L. Fogli *et al.*, Prog. Part. Nucl. Phys. **57**, 742 (2006).